Fault-Tolerant Control Strategies of Five-Phase Induction Motor Drives under Open-Switch Fault

Fault-Tolerant Control Strategies of Five-Phase Induction Motor Drives under Open-Switch Fault

L. Vancini, M. Mengoni, G. Rizzoli, L. Zarri, A. Tani

***Abstract* – When an open switch fault occurs, a power switch in a converter leg is always open while the corresponding freewheeling diode can still conduct. This type of fault is usually caused by some problems in the driver circuits or the PWM communication system.**

An open-switch fault is usually treated as an open-phase fault, but new control strategies with improved performance can be developed specifically for this type of fault.

In this paper, four different control strategies against an open switch fault are presented and compared in terms of stator Joule losses and torque ripple. A motor control scheme for multiphase induction motor drives is developed and assessed.

The feasibility of the proposed solution is verified by means of experimental tests on a prototype of five-phase induction motor.

***Index Terms*- Multiphase machines, Induction motor drives, Fault-tolerant control.**

I. Introduction

Multiphase ac machines and multiphase inverters are feasible solutions in critical applications to increase fault tolerance [1] - [3].

The larger number of degrees of freedom of multiphase drives compared to the three-phase ones can be exploited in different ways.

The first way is to improve the torque density. In multiphase machines, the spatial harmonic components of the magnetic field in the airgap can be controlled independently. In motors with concentrated windings, if the third spatial harmonic is synchronized with the fundamental one, the torque capability of the machine increases, resulting in motor drives with high-torque density [4] - [7].

Another possibility is to use the degrees of freedom to diagnose the health status of multiphase machines.

For example, high-resistance connections can be detected and located [8] - [11]. This problem can be caused by mechanical stress, thermal cycling, or the chemical corrosion of electrical connections. These conditions can lead to local overheating and unbalanced motor supply voltages, affecting system performance, efficiency, and reliability.

The inter-turn short circuit is another severe fault condition in electrical machines. Usually, only a few turns are affected by this fault, making the diagnosis a difficult task. Nonetheless, this fault can be potentially destructive, creating hot spots that may irreparably damage the motor. Only a few papers have analyzed this type of fault in detail for multiphase machines [12] - [15].

However, among all the possible faults, one of the most studied in the literature is the open-phase fault. This fault often caused by damage to the power components or driver circuits of the inverter. Multiphase drives are inherently robust to phase faults, but the control systems must be able to effectively determine and promptly locate faults. The papers on this topic can be classified into contributions focused on fault detection [16] - [18] and contributions presenting fault-tolerant strategies [19] - [22].

Since it is implausible that two power switches placed in the same converter leg can fail simultaneously, most of open phase faults (OPFs) are actually open-switch faults (OSFs).

Usually, this situation is not analyzed in detail, and it is preferred to cut the power in the faulty phase, but the presence of a working freewheeling diode in the faulty switch could be exploited. After an OSF, the current in the faulty phase can only flow in one direction.

This work presents four different control strategies for OSF in five-phase induction motor drives.

The Vector Space Decomposition (VSD) is used to develop the fault-tolerant control technique and determine the analytical expression of the stator current in the healthy phases, ensuring disturbance-free operation and the minimum value of the stator copper losses under both transient and steady-state operating conditions.

This paper presents a control scheme for a five-phase induction motor based on resonant regulators capable of ensuring the motor operation during an OSF.

The manuscript is organized as follows. Section II illustrates the equations of a five-phase induction motor and includes the analysis of the motor based on the VSD. Section III describes four different fault-tolerant strategies for OSF and compare the performance in terms of stator Joule losses. Section IV presents the developed motor control scheme. Experimental results obtained with a five-phase induction motor drive are presented in Section VI. The experimental validation includes the analysis of the torque and line current waveform and confirms the feasibility of the proposed solutions.

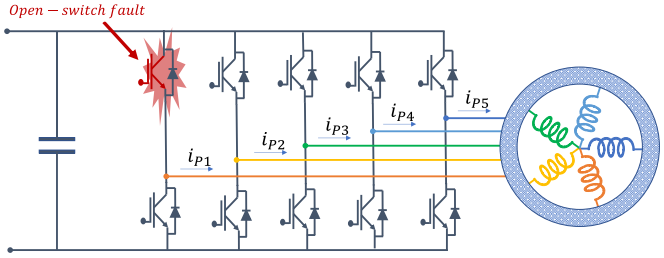

Fig. 1 – Open switch fault in a five-phase inverter.

L. Vancini, M. Mengoni, G. Rizzoli, L. Zarri, A. Tani are with Department of Electrical, Electronic and Information Engineering "Guglielmo Marconi", University of Bologna, Bologna 40136, Italy (e-mail: luca.vancini4@unibo.it, michele.mengoni@unibo.it, gabriele.rizzoli@unibo.it, luca.zarri2@unibo.it, angelo.tani@unibo.it).

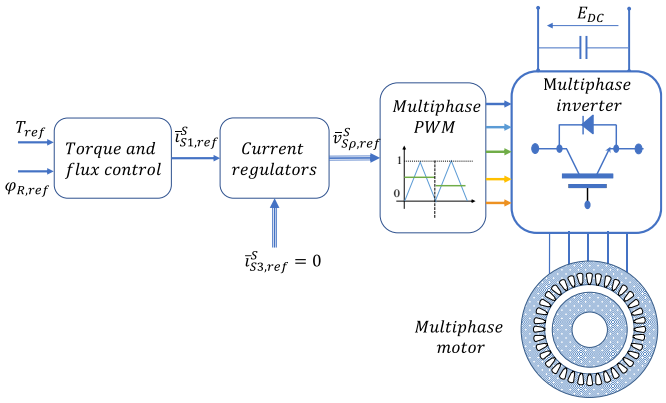

Fig. 2 – Qualitative scheme of a multiphase induction motor drive in healthy operating conditions.

II. Machine Equations

The study of multiphase machines uses the mathematical approach called Vector Space Decomposition (VSD). This transformation extends the Clarke transformation for systems with a phase number greater than three.

For a given set of 5 real variables $x_1, \dots, x_5$, a new set of complex variables $x_0, \bar{x}_1, \bar{x}_3$ can be obtained by means of the following symmetrical linear transformations:

$$x_0 = \frac{1}{5}\sum_{k=1}^{5} x_k \,, \qquad \bar{x}_\rho = \frac{2}{5}\sum_{k=1}^{5} x_k \, \bar{\alpha}^{\rho(k-1)} \,, \quad \rho = 1,3. \tag{1}$$

where $\bar{\alpha} = e^{j2\pi/5}$.

The inverse transformations of (1) are as follows:

$$x_k = x_0 + \sum_{\rho=1,3} \bar{x}_\rho \cdot \bar{\alpha}^{\rho(k-1)} \,, \quad k = 1,2,\dots,5 \tag{2}$$

where the symbol "·" represents the dot product, defined as the real part of the product between the first operand and the complex conjugate of the second.

According to the VSD, the model of a five-phase induction machine can be represented by the following set of complex equations in the fundamental and the third harmonic subspaces:

$$\bar{v}_{S1} = R_S \bar{\imath}_{S1} + j\omega_1 \bar{\varphi}_{S1} + \frac{d\bar{\varphi}_{S1}}{dt} \tag{3}$$

$$\bar{v}_{R1} = R_{R1} \bar{\imath}_{R1} + j(\omega_1 - \omega_m)\bar{\varphi}_{R1} + \frac{d\bar{\varphi}_{R1}}{dt} \tag{4}$$

$$\bar{\varphi}_{S1} = L_{S1} \bar{\imath}_{S1} + M_1 \bar{\imath}_{R1} \tag{5}$$

$$\bar{\varphi}_{R1} = M_1 \bar{\imath}_{S1} + L_{R1} \bar{\imath}_{R1} \tag{6}$$

$$\bar{v}_{S3} = R_S \bar{\imath}_{S3} + j\omega_3 \bar{\varphi}_{S3} + \frac{d\bar{\varphi}_{S3}}{dt} \tag{7}$$

$$\bar{v}_{R3} = R_{R3} \bar{\imath}_{R3} + j(\omega_3 - 3\omega_m)\bar{\varphi}_{R3} + \frac{d\bar{\varphi}_{R3}}{dt} \tag{8}$$

$$\bar{\varphi}_{S3} = L_{S3} \bar{\imath}_{S3} + M_3 \bar{\imath}_{R3} \tag{9}$$

$$\bar{\varphi}_{R3} = M_3 \bar{\imath}_{S3} + L_{R3} \bar{\imath}_{R3} \tag{10}$$

$$T_1 = \frac{5}{2} p(\bar{\imath}_{S1} \cdot j\bar{\varphi}_{S1} + 3\bar{\imath}_{S3} \cdot j\bar{\varphi}_{S3}) \tag{11}$$

where $\bar{v}_{S\rho}$ and $\bar{v}_{R\rho}$ $(\rho = 1,3)$ are the space vectors of the stator and rotor voltages, $\bar{\imath}_{S\rho}$ and $\bar{\imath}_{R\rho}$ $(\rho = 1,3)$ are the space vectors of the stator and rotor currents, $\bar{\varphi}_{S\rho}$ and $\bar{\varphi}_{R\rho}$ $(\rho = 1,3)$ are the space vectors of the stator and rotor fluxes, ω_m is the electric angular speed of the rotor, p is the number of pole pairs, $R_{R\rho}$ $(\rho = 1,3)$ are the rotor resistances and $L_{S\rho}$, $L_{R\rho}$ and M_ρ $(\rho = 1,3)$ are the self and mutual inductances of the stator and rotor windings. The stator resistance R_S is the same for all subspaces. The motor torque is the sum of the contributions generated in each subspace. Equations (3) - (6) and (7) - (10) are written respectively in the rotor-flux oriented reference frames $d_1 - q_1$ and $d_3 - q_3$ with angular speeds ω_1 and ω_3.

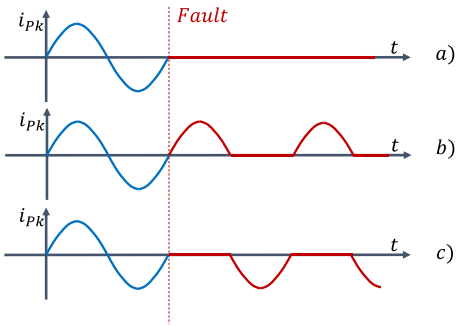

Fig. 3 – Stator current waveform of kth phase in open-circuit fault. Current waveform in open-phase fault a), current waveform in open-switch fault of the lower switch b) current waveform in open-circuit fault of the upper switch c).

The qualitative diagram of a current-regulated multiphase motor drive is depicted in Fig. 2. The reference value of the first current space vector, i.e., $\bar{\imath}^S_{S1,ref}$, is calculated by the control system to satisfy the demand for torque and flux, whereas the remaining current space vectors are usually set to zero. In this way, the airgap MMF has a sinusoidal distribution, the torque pulsation and the rotor losses are strongly reduced, and the stator copper losses are minimized.

III. Open Switch Fault

Open-circuit faults can be classified into open-phase faults (OPFs) and open-switch faults (OSFs). The OPFs can be caused by interruption of electrical continuity in the stator windings or accidental disconnection between the power converter and the electric motor. This fault forces a stator phase current to zero. Therefore, due to this constraint, the electrical machines affected by this issue undergo a power derating.

The OSFs are typically dependent on converter faults involving power switches or drivers. During this fault, the current conduction of the upper or lower power switch of a converter leg is no longer possible (Fig. 1). Anyway, the corresponding freewheeling diode is not affected by the fault and can conduct. Therefore, when an open switch fault occurs, the corresponding current can flow only in one direction. This constraint is slightly different from the one imposed by OPF because it depends on the stator current path. If the fault affects the upper switch, the corresponding output current can only have a negative sign. On the contrary, if the lower switch is faulty, the phase current can only be positive (Fig. 3). In other words, the corresponding inverter leg becomes a buck or boost leg, causing the current to flow in only one direction.

In both OPF and OSF situations, the general approach is to isolate the fault by zeroing the phase current and allowing the motor to operate with the remaining phases. This paper

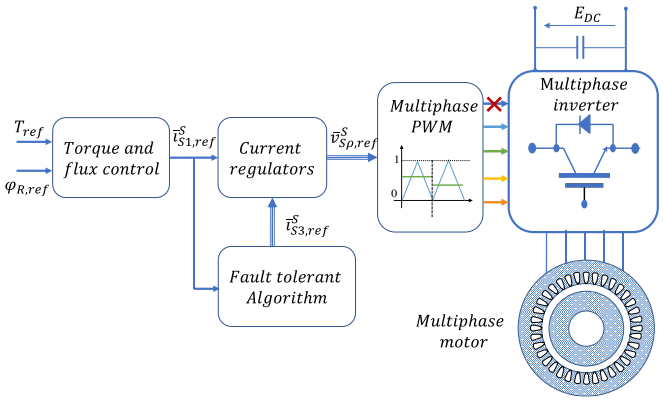

Fig. 4 – Qualitative scheme of a multiphase induction motor drive in faulty operating conditions.

presents alternative solutions that improve the motor performance by detecting the phase current sign.

During a fault of the lower power switch of kth phase, the corresponding stator phase currents have to satisfy the following constraint:

$$\begin{cases} if\ \bar{\imath}^S_{S1,ref} \cdot \bar{\alpha}^{(k-1)} > 0 \Rightarrow i_{Pk} = \bar{\imath}^S_{S1,ref} \cdot \bar{\alpha}^{(k-1)} \\ Otherwise\ \ i_{Pk} = \sum_{\rho=1,3} \bar{\imath}^S_{S\rho,ref} \cdot \bar{\alpha}^{\rho(k-1)} = 0 \end{cases} \quad (12)$$

where $\bar{\imath}^S_{S\rho,ref}$ is the ρth reference current space vector in the stationary reference frame. Equation (12) assumes that the reference current space vectors $\bar{\imath}^S_{S3,ref}$ is a degree of freedom that the control system can arbitrarily assign to manage the fault. In other words, (10) implies that $\bar{\imath}^S_{S3,ref}$ becomes a function of $\bar{\imath}^S_{S1,ref}$ when the reference current in the kth phase is negative. Since the reference space vector $\bar{\imath}^S_{S1,ref}$ is calculated by the control system to track the torque and the flux set points, (12) cannot be satisfied if $\bar{\imath}^S_{S3,ref}$ is null.

Similarly, (13) describes the constrain on the stator currents in the event of an upper switch fault.

$$\begin{cases} if\ \bar{\imath}^S_{S1,ref} \cdot \bar{\alpha}^{(k-1)} < 0 \Rightarrow i_{Pk} = \bar{\imath}^S_{S1,ref} \cdot \bar{\alpha}^{(k-1)} \\ Otherwise\ \ i_{Pk} = \sum_{\rho=1,3} \bar{\imath}^S_{S\rho,ref} \cdot \bar{\alpha}^{\rho(k-1)} = 0 \end{cases} \quad (13)$$

It is worth noting that disturbance-free operation can be achieved if the harmonic distribution of the Magneto Motive Force (MMF), produced by the stator phase windings in the air gap, does not change in pre and post-fault conditions. This stringent requirement can be satisfied only for machines with "sinusoidally" distributed stator windings. However, in the general case, it is possible to keep at least the first spatial harmonic undisturbed and preserve the reference space vector $\bar{\imath}^S_{S1,ref}$.

A disturbance-free control algorithm, which minimizes the instantaneous stator copper losses in steady-state and transient conditions, is developed in the next sections. Since $\bar{\imath}^S_{S1,ref}$ is calculated by the control system, the basic idea is to choose the remaining reference current space vector $\bar{\imath}^S_{S3,ref}$ in such a way to improve motor performance.

A. *Open-Phase Fault with Minimum Stator Joule Losses*

The first control strategy that is presented treats the OSF as an OPF. In this case, the line current of the faulty phase k is zeroed by the motor control system.

$$i_{Pk} = \sum_{\rho=1,3} \bar{\imath}^S_{S\rho} \cdot \bar{\alpha}^{\rho(k-1)} = 0 \quad (14)$$

Equation (12) leaves a degree of freedom that can be used to minimize stator Joule losses.

Under the assumption that the open-phase fault affects only the kth phase, the optimal instantaneous values of the current reference space vectors that ensure the minimum stator copper losses can be expressed in the stator reference frame as follows:

$$\bar{\imath}^S_{S3,ref} = -\bar{\alpha}^{3(k-1)}\left[\bar{\imath}^S_{S1,ref} \cdot \bar{\alpha}^{(k-1)}\right]. \quad (15)$$

A qualitative motor control scheme implementing the proposed fault-tolerant strategies is presented in Fig. 4.

In steady-state conditions, the current space vector $\bar{\imath}^S_{S1,ref}$ rotates on a circular trajectory with constant angular speed ω_1. With this strategy, when the upper switch of the first leg of the converter is open, the trajectory of $\bar{\imath}^S_{S3,ref}$ is a degenerate ellipse, i.e., a segment placed on the real axis (Fig. 5b). Therefore, the remaining four stator currents are sinusoidal and unbalanced, causing a nonuniform distribution of the stator copper losses among the stator windings. Furthermore, the stator Joule losses increase because the current amplitude rises to keep the motor torque unchanged. This increase depends on the magnetizing current and the requested motor torque.

Among all the strategies for OPF, this solution guarantees the minimum stator copper losses. However, in the case of OSF, alternative control strategies can be formulated to further improve the effectiveness of the fault tolerant control.

B. *Open-Switch Fault with Minimum Stator Joule Losses*

This strategy is very similar to the one presented in previous Section, but instead of zeroing a phase current completely, it allows the unidirectional flow of the stator current in the faulty phase. In other words, the freewheeling diode of the faulty switch is used to reduce the disturbance caused by the fault.

In fact, when the freewheeling diode is forward biased, the five-phase induction motor operates in healthy condition without torque disturbances or additional Joule losses. Conversely, when the diode is reverse biased, the line current is zeroed.

When the lower or the upper switch of kth converter leg is faulty, this control strategy is described respectively by (16) or (17).

$$\begin{cases} if\ \bar{\imath}^S_{S1,ref} \cdot \bar{\alpha}^{(k-1)} > 0 \Rightarrow \bar{\imath}^S_{S3,ref} = 0 \\ Otherwise\ \ \bar{\imath}^S_{S3,ref} = -\bar{\alpha}^{3(k-1)}\left[i^S_{S1,ref} \cdot \bar{\alpha}^{(k-1)}\right] \end{cases} \quad (16)$$

$$\begin{cases} if\ \bar{\imath}^S_{S1,ref} \cdot \bar{\alpha}^{(k-1)} < 0 \Rightarrow \bar{\imath}^S_{S3,ref} = 0 \\ Otherwise\ \ \bar{\imath}^S_{S3,ref} = -\bar{\alpha}^{3(k-1)}\left[i^S_{S1,ref} \cdot \bar{\alpha}^{(k-1)}\right] \end{cases} \quad (17)$$

Fig. 5c shows the trajectories of $\bar{\imath}^S_{S1,ref}$ and $\bar{\imath}^S_{S3,ref}$ in steady state conditions when the upper switch of first leg of the converter is open.

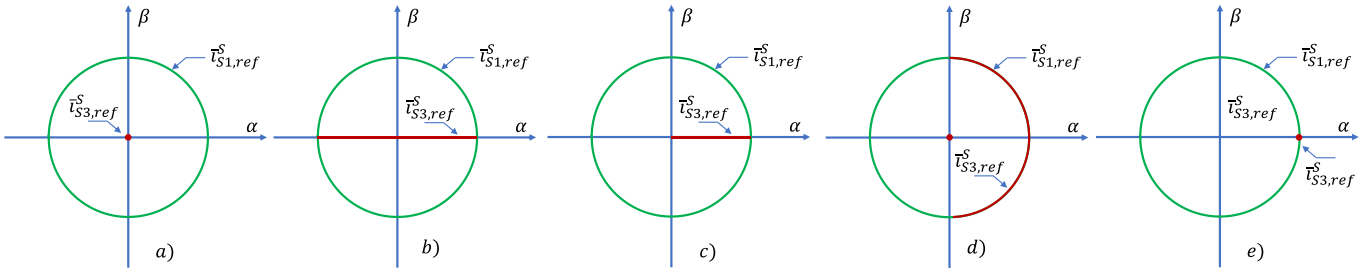

Fig. 5 – Trajectories of the stator current space vectors in five-phase induction motor with open-switch fault. Healthy motor a). OPF with minimum stator Joule losses b). Open switch fault with minimum stator Joule losses c). Semicircular trajectory d). DC Injection e).

Compared to the previous solution, this one reduces the stator copper losses by decreasing the RMS value of the line currents [19]. However, if the stator windings are not sinusoidally distributed, this strategy, as in the previous one, could lead to low-frequency torque pulsations.

C. *Semicircular Trajectory*

In order to eliminate these torque pulsations in fault conditions, counter-rotating stator magneto-motive force components should be avoided. This result can be obtained by forcing the current space vectors $\bar{\imath}^S_{S1,ref}$ and $\bar{\imath}^S_{S3,ref}$ to move along semicircular trajectories, with constant angular speed, as can be seen in Fig. 5d.

Among all strategies able to achieve this behavior, the one with the lowest stator Joule losses is defined by the following relationships:

$$\begin{cases} if\ \bar{\imath}^S_{S1,ref}\cdot\bar{\alpha}^{(k-1)} > 0 \Rightarrow \bar{\imath}^S_{S3,ref} = 0 \\ Otherwise\ \ \bar{\imath}^S_{S3,ref} = -\bar{\imath}^S_{S1,ref}\bar{\alpha}^{2(k-1)} \end{cases} (lower\ switch) \tag{18}$$

$$\begin{cases} if\ \bar{\imath}^S_{S1,ref}\cdot\bar{\alpha}^{(k-1)} < 0 \Rightarrow \bar{\imath}^S_{S3,ref} = 0 \\ Otherwise\ \ \bar{\imath}^S_{S3,ref} = -\bar{\imath}^S_{S1,ref}\bar{\alpha}^{2(k-1)} \end{cases} (upper\ switch) \tag{19}$$

The previous equations describe the current constrains of the strategy with the minimum torque pulsation when the lower or the upper switch of *k*th converter leg is faulty.

The results of this solution are shown in Fig. 5d. Unfortunately, the waveform of current $\bar{\imath}^S_{S3,ref}$ is discontinuous. Therefore, a high bandwidth of the current regulators and a significant voltage margin in the DC bus are required to track the current and suppress the torque oscillations. For these reasons, although theoretically correct, this solution does not provide satisfactory results in practical applications.

All fault-tolerant control strategies should avoid discontinuities in the trajectories of the current space vectors.

D. *DC injection with minimum torque pulsation*

The use of a direct current is another solution that cancels the oscillations of the torque and avoids the occurrence of discontinuities in the current setpoints [23].

The basic idea of this method is to include a DC component in $\bar{\imath}^S_{S3,ref}$ to ensure that the current is unidirectional in the faulty phase. The stator currents no longer have an average zero value, and the line current of the faulty phase is strictly positive or negative depending on the position of the faulty switch. This solution is probably the simplest but leads to the largest imbalance in copper losses among the stator phases.

Based on this control strategy, when the lower or the upper switch of *k*th converter leg is fault, this control strategy is described respectively by (20) or (21).

$$\bar{\imath}^S_{S3,ref} = -\left|\bar{\imath}^S_{S1,ref}\right|\bar{\alpha}^{3(k-1)} \tag{20}$$

$$\bar{\imath}^S_{S3,ref} = \left|\bar{\imath}^S_{S1,ref}\right|\bar{\alpha}^{3(k-1)}. \tag{21}$$

It is worth noting that this solution is still valid during current transients caused by torque or speed transient.

In steady-state operating conditions, this control strategy causes the current space vectors to have an equal magnitude and $\bar{\imath}^S_{S3,ref}$ to be constant over time (Fig. 5e).

E. *Stator Joule Losses of Fault Tolerant Strategies*

The fault-tolerant strategies described in the previous sections in case of a faulty phase have been compared, in steady-state operating conditions, in terms of stator copper losses.

The instantaneous stator copper losses can be calculated as follows:

$$P_{JS} = R_s\sum_{k=1}^{5} i^2_{Pk}(t) \tag{22}$$

Expressing the currents in (22) in terms of space vectors leads to the following result:

$$P_{JS} = \frac{5}{2}R_s\sum_{\rho=1,3}\left|\bar{\imath}^S_{S\rho}\right|^2. \tag{23}$$

Taking (15) – (21) into account and considering constant $|\bar{\imath}_{S1}|$, it can be demonstrated that:

$$P_{JS,OPF} = \frac{3}{2}P_{JS,healthy} \tag{24}$$

$$P_{JS,OSF\ min\ loss} = \frac{5}{4}P_{JS,healthy} \tag{25}$$

$$P_{JS,Semicirc} = \frac{3}{2}P_{JS,healthy} \tag{26}$$

$$P_{JS,DC\ inj} = \frac{7}{4}P_{JS,healthy}. \tag{27}$$

As can be seen, the best strategy is (25), whereas the worst one is (27).

In the case of "sinusoidally" distributed stator windings, only the stator copper losses should be considered because the rotor quantities are the same as in healthy conditions. In the case of non-sinusoidally distributed stator windings, the comparison in terms of rotor copper losses, average torque, and torque ripple depends on the operating conditions and is strongly affected by the stator winding distribution. In other

words, if the fault tolerant strategy univocally determines the stator Joule losses, the rotor and the iron losses are strictly dependent on the motor operating point and the motor parameters.

IV. Motor Control Scheme

The block diagram of the control system, based on a conventional rotor-flux oriented control scheme in the fundamental subspace, is shown in Fig. 6. The rotor speed is adjusted by Proportional Integral (PI) regulator (a), while the currents $i_{S1d,ref}$ and $i_{S1q,ref}$ are tracked by PI regulators (c) and (b). For simplicity, the reference value $i_{S1d,ref}$ is constant and equal to the motor magnetizing current, but the field weakening capability can be obtained with some additional control loops. For the proper behavior of the control system, an anti-windup scheme is adopted in order to prevent the saturation of PI regulator (a). As a consequence, the maximum value of $i_{S1q,ref}$ is limited by $i_{S1d,ref}$ and the amplitude of the other current space vector $\bar{\imath}_{S3,ref}$.

The quantity I_{max} is the maximum RMS value of the stator phase current.

When the motor is healthy, the setpoint of reference current $\bar{\imath}_{S3,ref}$ is zero. However, when a fault is detected, new setpoint values are determined according to the fault-tolerant strategies outlined in the previous sections.

Unfortunately, in fault operating conditions, the reference signals of the stator currents can contain a remarkable inverse sequence component at angular frequency $-\omega_1$, which leads to a relevant distortion of the waveforms.

The presence of harmonics at frequencies ω_1 and $-\omega_1$ in the reference signals can be easily solved by using resonant PI regulators (PIRs). Therefore, the current reference $\bar{\imath}_{S3,ref}$ is tracked by PIR (d) and (e) implemented in the stationary reference frame $\alpha_3 - \beta_3$.

In the case of DC injection only, the use of PIRs is not necessary and simple PI regulators are sufficient.

The estimation of the rotor flux $\bar{\varphi}_{R1}^{S}$ is necessary for the field-oriented control both in healthy and fault operating conditions. The observer adopted in this paper is based on the rotor equations and the measurements of the rotor speed and stator currents.

TABLE I
PARAMETERS OF THE FIVE-PHASE MACHINE

$E_{DC} = 150\ V$	$I_{S1,max} = 7\ A$	$p = 3$
$L_{S1} = 411\ mH$	$L_{S3} = 68\ mH$	$M_1 = 555\ mH$
$L_{R1} = 939\ mH$	$L_{R3} = 158\ mH$	$M_3 = 53\ mH$
$R_S = 1.7\ \Omega$	$R_{R1} = 4.8\ \Omega$	$R_{R3} = 4.8\ \Omega$

Finally, the PWM block calculates the gate signals of the five inverter legs by using a five-phase space vector PWM technique [1].

V. Experimental Results

Some experimental tests performed on a five-phase induction motor, whose parameters are listed in Table I, have confirmed the performance of the developed fault-tolerant strategies.

Preliminary experimental tests in steady-state conditions have been carried out with a torque reference of 10 Nm and a rotor speed of about 150 rpm. The results obtained in healthy conditions are presented in Figs. 7a and 8a. As expected, the stator currents are balanced and sinusoidal. In steady state conditions, the current space vector $\bar{\imath}_{S1}$ in healthy or in fault conditions moves along a circular trajectory. The torque waveform, measured by a torque meter, and its spectrum are illustrated in Fig. 9a. As can be seen, the torque is practically constant. The only harmonic components are minimal on the logarithmic scale and are due to mechanical causes.

As can be seen in Figs. 7b and 8b, the OPF strategy with the minimum stator copper losses leads to sinusoidal and unbalanced stator currents, and the torque behavior is characterized by a torque ripple with a frequency twice that of the currents (Fig. 9b). The current space vector $\bar{\imath}_{S3}$ moves along a segment while the trajectory of $\bar{\imath}_{S1}$ remains practically unchanged compared to the healthy motor.

The OSF strategy with the minimum stator copper losses is illustrated in Figs. 7c and 8c. The phase currents remain unbalanced, but their RMS value is significantly lower compared to the previous case. The main harmonic component of the torque ripple is at frequency f_1, while the component at twice the base frequency is attenuated compared to the previous case (Fig. 9c).

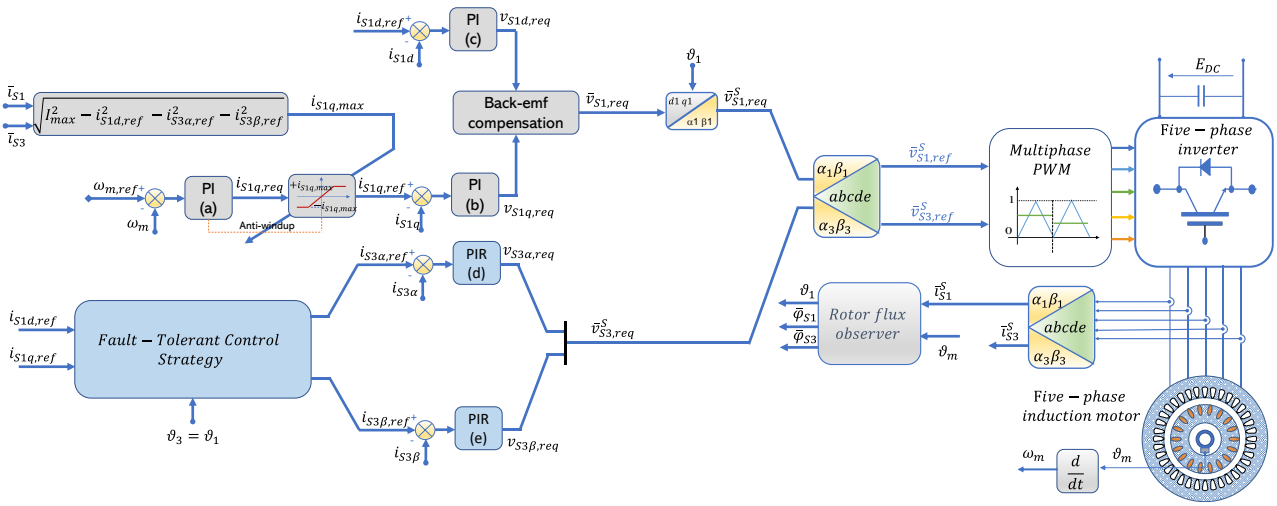

Fig. 6 – Motor control scheme.

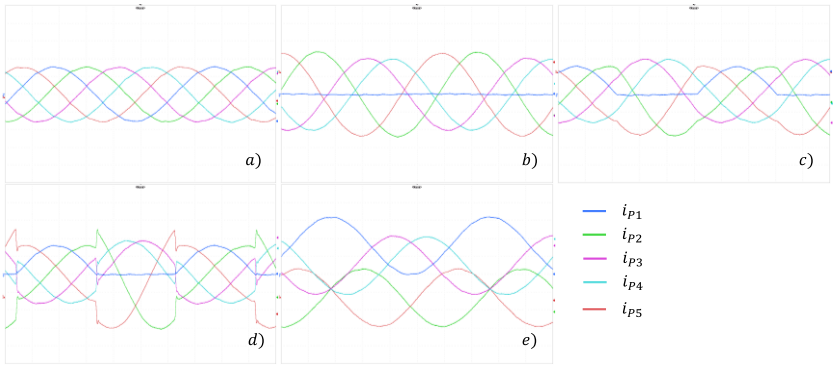

Fig. 7 – Experimental results. Waveforms of stator phase currents (2 A/div) in healthy conditions a), OPF with minimum stator Joule losses b), OSF with minimum stator Joule losses c), semicircular trajectory d), and DC injection e).

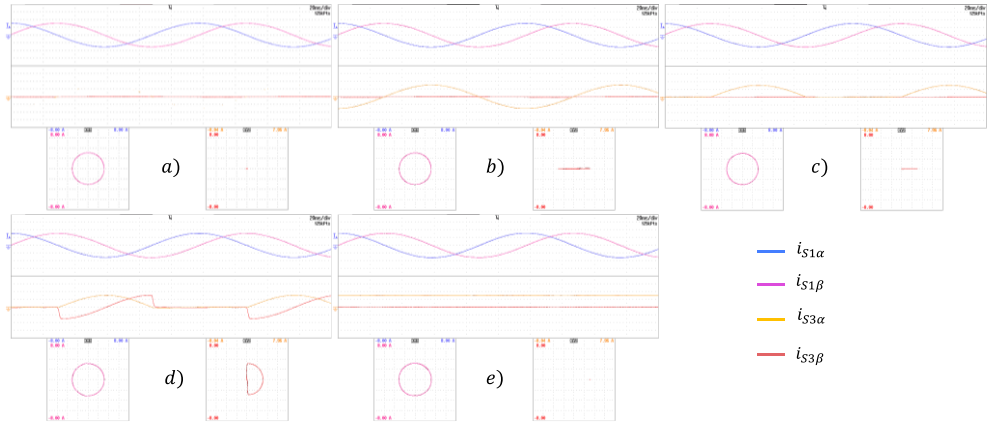

Fig. 8 – Experimental results. Waveforms and trajectories of stator current space vector $\bar{\imath}_{S1}$ and $\bar{\imath}_{S3}$ (2 A/div) in healthy conditions a), OPF with minimum stator Joule losses b), OSF with minimum stator Joule losses c), semicircular trajectory d), and DC injection e).

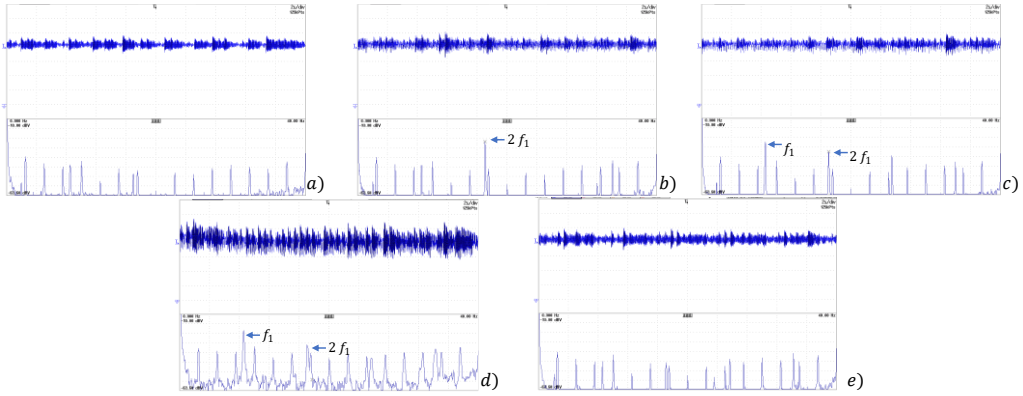

Fig. 9 – Experimental results. Torque waveforms (2.5 Nm/div) and harmonic spectrum (33 dB Nm/div) in healthy conditions a), OPF with minimum stator Joule losses b), OSF with minimum stator Joule losses c), semicircular trajectory d), and DC injection e).

Figs. 7d and 8d show the current waveform of the strategy with a semicircular trajectory and as expected, there are discontinuities. This behavior is very stressful for the current regulators, which must therefore have a high bandwidth.

The difficulty of tracking the current setpoints causes many oscillations in waveform of the torque (Fig. 9d). In conclusion, this solution has the worst torque performance.

The effects of DC injection are shown in Figs. 7e and 8e. Obviously, although the line currents do not have discontinuities, they have a non-zero average value. The current space vector $\bar{\imath}_{S3}$ is a fixed point in the plane $\alpha_3 - \beta_3$.

The RMS of line current is greater than the previous solutions and the imbalance of Joule losses among the phases is very high. However, the torque waveform is very similar to that of the healthy machine (Fig. 9e).

VI. Conclusions

In this paper, a control scheme and four fault-tolerant strategies for five-phase induction motor drives are presented. The OSF is analyzed and compared with the OPF.

The theoretical analysis shows that it is possible to increase motor efficiency and reduce the torque ripple by distinguishing these two types of faults.

The analytical formulation of these fault-tolerant control strategies represents the multiphase variables as multiple space vectors and is valid in both steady-state and transient operation.

A control scheme based on resonant controllers has been proposed. The PIR controllers can be used to adjust the phase

voltage to track different current trajectories in the complex plane.

Experimental tests have confirmed the correctness of the theoretical analysis and the feasibility of the control scheme. The developed fault-tolerant strategy can improve the efficiency and reliability of multiphase drives.

VII. REFERENCES

[1] M. J. Duran and F. Barrero, "Recent Advances in the Design, Modeling, and Control of Multiphase Machines—Part II," in IEEE Transactions on Industrial Electronics, vol. 63, no. 1, pp. 459-468, Jan. 2016.

[2] L. Parsa and H. A. Toliyat, "Fault-Tolerant Interior-Permanent-Magnet Machines for Hybrid Electric Vehicle Applications," in IEEE Transactions on Vehicular Technology, vol. 56, no. 4, pp. 1546-1552, July 2007.

[3] W. Cao, B. C. Mecrow, G. J. Atkinson, J. W. Bennett and D. J. Atkinson, "Overview of Electric Motor Technologies Used for More Electric Aircraft (MEA)," in IEEE Transactions on Industrial Electronics, vol. 59, no. 9, pp. 3523-3531, Sept. 2012.

[4] M. Mengoni, L. Zarri, A. Tani, L. Parsa, G. Serra and D. Casadei, "High-Torque-Density Control of Multiphase Induction Motor Drives Operating Over a Wide Speed Range," in IEEE Transactions on Industrial Electronics, vol. 62, no. 2, pp. 814-825, Feb. 2015.

[5] K. Wang, "Effects of Harmonics into Magnet Shape and Current of Dual Three-Phase Permanent Magnet Machine on Output Torque Capability," in IEEE Transactions on Industrial Electronics, vol. 65, no. 11, pp. 8758-8767, Nov. 2018.

[6] A. S. Abdel-Khalik, M. I. Masoud and B. W. Williams, "Improved Flux Pattern with Third Harmonic Injection for Multiphase Induction Machines," in IEEE Transactions on Power Electronics, vol. 27, no. 3, pp. 1563-1578, March 2012.

[7] I H. Chen, J. He, X. Guan, N. A. O. Demerdash, A. M. EL-Refaie and C. H. T. Lee, "High-Resistance Connection Diagnosis in Five-Phase PMSMs Based on the Method of Magnetic Field Pendulous Oscillation and Symmetrical Components," in IEEE Transactions on Industrial Electronics, vol. 69, no. 3, pp. 2288-2299, March 2022.

[8] J. Hang, X. Ren, C. Tang, M. Tong and S. Ding, "Fault-Tolerant Control Strategy for Five-Phase PMSM Drive System with High-Resistance Connection," in IEEE Transactions on Transportation Electrification, vol. 7, no. 3, pp. 1390-1400, Sept. 2021.

[9] P. F. C. Gonçalves, S. M. A. Cruz and A. M. S. Mendes, "Online Diagnostic Method for the Detection of High-Resistance Connections and Open-Phase Faults in Six-Phase PMSM Drives," in IEEE Transactions on Industry Applications, vol. 58, no. 1, pp. 345-355, Jan.-Feb. 2022.

[10] M. Mengoni et al., "Online Detection of High-Resistance Connections in Multiphase Induction Machines," in IEEE Transactions on Power Electronics, vol. 30, no. 8, pp. 4505-4513, Aug. 2015.

[11] F. Wu, P. Zheng and T. M. Jahns, "Analytical Modeling of Interturn Short Circuit for Multiphase Fault-Tolerant PM Machines with Fractional Slot Concentrated Windings," in IEEE Transactions on Industry Applications, vol. 53, no. 3, pp. 1994-2006, May-June 2017.

[12] F. Wu, A. M. EL-Refaie and P. Zheng, "Diagnosis and Remediation of Single-Turn Short Circuit in a Multiphase FSCW PM Machine Based on T-type Equivalent Circuit," in IEEE Transactions on Industry Applications, vol. 56, no. 1, pp. 158-169, Jan.-Feb. 2020.

[13] F. Immovilli, C. Bianchini, E. Lorenzani, A. Bellini and E. Fornasiero, "Evaluation of Combined Reference Frame Transformation for Interturn Fault Detection in Permanent-Magnet Multiphase Machines," in IEEE Transactions on Industrial Electronics, vol. 62, no. 3, pp. 1912-1920, March 2015.

[14] Y. Fan, C. Li, W. Zhu, X. Zhang, L. Zhang and M. Cheng, "Stator Winding Interturn Short-Circuit Faults Severity Detection Controlled by OW-SVPWM Without CMV of a Five-Phase FTFSCW-IPM," in IEEE Transactions on Industry Applications, vol. 53, no. 1, pp. 194-202, Jan.-Feb. 2017.

[15] I. González-Prieto, M. J. Duran, N. Rios-Garcia, F. Barrero and C. Martín, "Open-Switch Fault Detection in Five-Phase Induction Motor Drives Using Model Predictive Control," in IEEE Transactions on Industrial Electronics, vol. 65, no. 4, pp. 3045-3055, April 2018.

[16] M. J. Duran, I. Gonzalez-Prieto, N. Rios-Garcia and F. Barrero, "A Simple, Fast, and Robust Open-Phase Fault Detection Technique for Six-Phase Induction Motor Drives," in IEEE Transactions on Power Electronics, vol. 33, no. 1, pp. 547-557, Jan. 2018.

[17] P. Garcia-Entrambasaguas, I. González-Prieto and M. J. Duran, "Single-Index Open-Phase Fault Detection Method for Six-Phase Electric Drives," in IEEE Transactions on Industrial Electronics, vol. 67, no. 12, pp. 10233-10242, Dec. 2020.

[18] A. Tani, M. Mengoni, L. Zarri, G. Serra and D. Casadei, "Control of Multiphase Induction Motors with an Odd Number of Phases Under Open-Circuit Phase Faults," in IEEE Transactions on Power Electronics, vol. 27, no. 2, pp. 565-577, Feb. 2012.

[19] H. S. Che, M. J. Duran, E. Levi, M. Jones, W. Hew and N. A. Rahim, "Postfault Operation of an Asymmetrical Six-Phase Induction Machine with Single and Two Isolated Neutral Points," in IEEE Transactions on Power Electronics, vol. 29, no. 10, pp. 5406-5416, Oct. 2014.

[20] S. Dwari and L. Parsa, "An Optimal Control Technique for Multiphase PM Machines Under Open-Circuit Faults," in IEEE Transactions on Industrial Electronics, vol. 55, no. 5, pp. 1988-1995, May 2008.

[21] F. Baneira, J. Doval-Gandoy, A. G. Yepes, Ó. López and D. Pérez-Estévez, "Control Strategy for Multiphase Drives with Minimum Losses in the Full Torque Operation Range Under Single Open-Phase Fault," in IEEE Transactions on Power Electronics, vol. 32, no. 8, pp. 6275-6285, Aug. 2017.

[22] J. Sun, Z. Zheng, C. Li, K. Wang and Y. Li, "Optimal Fault-Tolerant Control of Multiphase Drives Under Open-Phase/Open-Switch Faults Based on DC Current Injection," in IEEE Transactions on Power Electronics, vol. 37, no. 5, pp. 5928-5936, May 2022.

VIII. BIOGRAPHIES

L. Vancini received the M.Sc. degree in electrical engineering in 2018 from the University of Bologna, Bologna, Italy, where he is currently working toward the Ph.D. degree in electrical engineering with the Department of Electric, Electronic and Information Engineering "Guglielmo Marconi." His research interests include power electronics, control of multiphase converters, and diagnostic techniques for multiphase machines.

M. Mengoni received the M.Sc. and Ph.D. degrees in electrical engineering from the University of Bologna, Bologna, Italy, in 2006 and 2010, respectively. He is currently an Associate Professor with the Department of Electric, Electronic and Information Engineering "Guglielmo Marconi," University of Bologna. His research interests include the design, analysis, and control of three-phase electric machines, multiphase drives, and ac/ac matrix converters.

G. Rizzoli received the M.Sc. and Ph.D. degrees in electrical engineering from the University of Bologna, Bologna, Italy, in 2012 and 2016, respectively. In 2015, he was a Visiting Student with Virginia Tech (CPES), Blacksburg, VA, USA. He is currently an Assistant Professor with the Department of Electrical, Electronic and Information Engineering "Guglielmo Marconi," University of Bologna. His research interests include the design of electrical machines, the development and control of high-efficient power converters for automotive and renewable energy applications.

L. Zarri (Senior Member, IEEE) received the M.Sc. and Ph.D. degrees in electrical engineering from the University of Bologna, Bologna, Italy, in 1998 and 2007, respectively. He is currently a Full Professor of Power Electronics, Electrical Machines and Drives at the Department of Electrical, Electronic and Information Engineering "Guglielmo Marconi," University of Bologna. He has authored or co-authored more than 170 scientific papers. His research activity concerns the control of power converters and electric drives. Dr. Zarri is a senior member of the IEEE Industry Applications, Power Electronics, and Industrial Electronics societies.

A. Tani received the M.Sc. (Hons.) degree in electrical engineering from the University of Bologna, Bologna, Italy, in 1988. He is currently a Full Professor of power electronics, electrical machines and drives with the Department of Electrical, Electronic and Information Engineering "Guglielmo Marconi," University of Bologna. He has authored more than 200 papers published in technical journals and conference proceedings. His current activities include modeling, control, and fault diagnosis of multiphase electric machines.